



HAL
open science

Experimental study of bending behaviour of reinforcements

Emmanuel de Bilbao, D. Soulat, G. Hivet, Alain Gasser

► **To cite this version:**

Emmanuel de Bilbao, D. Soulat, G. Hivet, Alain Gasser. Experimental study of bending behaviour of reinforcements. *Experimental Mechanics*, 2010, 50 (3), pp.333-351. 10.1007/s11340-009-9234-9 . hal-00649570

HAL Id: hal-00649570

<https://hal.science/hal-00649570>

Submitted on 8 Dec 2011

HAL is a multi-disciplinary open access archive for the deposit and dissemination of scientific research documents, whether they are published or not. The documents may come from teaching and research institutions in France or abroad, or from public or private research centers.

L'archive ouverte pluridisciplinaire **HAL**, est destinée au dépôt et à la diffusion de documents scientifiques de niveau recherche, publiés ou non, émanant des établissements d'enseignement et de recherche français ou étrangers, des laboratoires publics ou privés.

1 **Experimental study of bending behaviour of reinforcements**

2 **E. de Bilbao · D. Soulat · G. Hivet · J.**

3 **Launay · A. Gasser**

4

5 Received: date / Revised version: date

6 **Abstract** In composite reinforcement shaping, textile preform undergo biaxial ten-
7 sile deformation, in plane shear deformation, transverse compaction and out-of-plane
8 bending deformations. Up today, bending deformations are neglected in some simu-
9 lation codes but taking into account them would give more accurate simulations of
10 forming especially for stiff and thick textiles. Bending behaviour is specific because
11 the reinforcements are structural parts and out of plane properties cannot be directly
12 deduced from in-plane properties, like continuous material. Because the standard tests
13 are not adapted for stiff reinforcements with non linear behaviour a new flexometer
14 using optical measurements has been developed to test such reinforcements. This new
15 apparatus enables to carry out a set of cantilever tests with different histories of load.
16 A series of tests has been performed to validate the test method and to show the
17 capacities of the new flexometer to identify non linear non elastic behaviour.

Send offprint requests to: emmanuel.debilbao@univ-orleans.fr

Institut PRISME/MMH - University of Orléans.

Polytech'Orléans. 8 rue Leonard de Vinci, 45072 ORLEANS Cedex 2, France.

E-mail: emmanuel.debilbao@univ-orleans.fr

18 **Keywords** Composite reinforcement – Carbon fabrics – Bending behaviour –
19 Experimental characterization

20 **1 Introduction**

21 Composite parts contain resin and can be constituted with short or long fibers [1].
22 For structural applications, long fibers and continuous reinforcements are generally
23 used which give to the piece the mechanical properties and the resin function is to re-
24 strain the motion of the yarns. Their use is increasing in automotive construction and
25 above all in aeronautics for structural parts. Such reinforcements allow to manufacture
26 composite structures with complex shapes for example by the RTM (Resin Transfer
27 Molding) process. The first stage of this process consists in a shaping of the dry woven
28 preform before resin injection [2, 3, 4]. In prepreg draping [2] or in continuous fibre rein-
29 forcements and thermo-plastic resin (CFRTP) forming [5, 6], the matrix is present but
30 is not hardened and the deformation of the structure is driven by those of the woven
31 reinforcement. Textile reinforcements are especially efficient in case of double curve
32 geometries because of the interlacing of warp and weft yarns. These geometries are
33 difficult to obtain with unidirectional reinforcements. To reach double curve geometry,
34 in-plane strains of the fabric are necessary. Because there are usually two directions
35 of yarns (warp and weft) that are interwoven, the fabric can reach very large in-plane
36 shear strain.

37 At the end of the first stage of the RTM process the fibers orientation and the local
38 variations of fiber volume fraction due to draping can have significant effect on the
39 mold filling process [7, 8, 9]. Moreover, the orientation of reinforcement fibers within
40 the preform will be a major factor in determining the structural properties of the fin-

41 ished piece [10, 11, 12]. The prediction of the deformability of the fabric during forming,
42 by simulation tool is essential for the understanding of the manufacture process and to
43 reduce product development cycle times and cost. In order to determine the deformed
44 shape of draped fabrics, several codes have been developed based on geometrical ap-
45 proaches so called fishnet algorithms [7, 13, 14, 15]. The alternative to these geometrical
46 methods consists of a mechanical analysis of the fabric deformation under the boundary
47 conditions prescribed by the forming process. This requires a model of the woven rein-
48 forcement and its mechanical behaviour, in order to compute the deformation through
49 a numerical method, for instance, the Finite Element Method.

50 In one of these methods [16, 17, 18, 19, 20] specific finite elements are defined that are
51 made of a discrete number of woven unit cells. The mechanical behaviour of these wo-
52 ven cells is obtained essentially by experimental analyses of the woven reinforcement.
53 Textile preforms undergo biaxial tensile deformations, in plane shear deformations,
54 transverse compaction and out-of-plane bending deformations. If all these deformations
55 can be significant in some cases it is generally possible to use a simplified approach
56 where only some strain energies are taken into account. The in plane shear strains are
57 necessary for woven reinforcement forming on a double curvature surface. The shear
58 angles can be very large (up to 50°) while the tensile strains remain small (1.5% for a
59 carbon fabric) [21]. In several approach bending behaviour is neglected but when the
60 forming stage leads to the formation of defaults, like wrinkles, taking into account out
61 of plane deformation, like the bending behaviour, could make more effective these sim-
62 ulation methods [22]. Wang et al. [23] demonstrated the relative importance of bending
63 behaviour during composite forming by comparison between bending and shear ener-
64 gies in case of viscous composites.

65 Moreover, it has been shown that bending properties cannot be deduced from in-plane

66 properties, like continuous material [24]. Reinforcement bending behaviour is a specific
67 structural out of plane behaviour. It depends, among other things, on the geometrical
68 configuration of the yarns, their mechanical properties, and the contact behaviour. The
69 determination of the specific bending behaviour of woven reinforcement, at macroscopic
70 scale, is an objective of this study. This determination consists in defining a functional
71 model. Macroscopic parameters of this model could be determined with bending tests
72 using direct identification or inverse method. Thereby, the experimental bending test of
73 composite reinforcements is necessary. The deformation behaviour of textiles has been
74 studied since a long time, by experimental approaches and by development of models.
75 Even if these studies concerning deformation of woven fabrics have been realized for
76 the clothing industry, especially in our case for the bending, we will apply in this paper
77 the methodology for the studied composite reinforcements.

78 So and since Peirce's model [25], many studies have been made to present analytical
79 model forecasting the bending behaviour of a fabric from the yarn properties and the
80 weave geometry in the field of clothing textiles. But these studies concern essentially
81 plain-woven fabrics. At present, it is not possible to predict accurately the bending
82 behaviour from only yarn properties for composite reinforcements with more complex
83 structures such as multiplies, interlock and 3D reinforcements or non crimp fabrics.

84 For experimental aspects, two standard tests are used to determine the bending stiff-
85 ness of fabrics: the standard cantilever test [26,27] and the Kawabata bending test
86 (KES-FB) [28]. The first is based on elastic linear behaviour and enables to determine
87 only one parameter: the bending rigidity. However the bending behaviour is not linear
88 elastic and the standard cantilever test is not adapted. The second test was designed
89 by Kawabata and enables to record the moment versus the curvature during a bending
90 cycle. Whereas it enables to show a non linear and hysteresis behaviour, it has been

91 designed to test clothing textiles and is not very well adapted for composite reinforce-
92 ments which are often thicker and stiffer and cannot be tested on this apparatus.
93 The purpose of this paper is to present a bending test for composite reinforcements
94 with various thicknesses. In this aim, a new cantilever test using optical measurements
95 has been designed. The sample can be either a yarn, a monopy or a multiply reinforce-
96 ment which cannot be tested with standard apparatus. The bending test is performed
97 for several overhang lengths which allow to identify non elastic behaviour. The test
98 results are the shapes of the bent samples for the different lengths and the moment
99 versus curvature curve. Associated to these experimental developments, we could de-
100 duce that macroscopic model for bending developed for clothing textiles are not very
101 adapted for the composite reinforcement.

102 **2 Reinforcements structure and properties**

103 2.1 Structure and in-plane properties

104 As explained in the introduction, dry reinforcements studied here are composed with
105 continuous yarns which contain thousands of fibers [29]. To allow the shaping into
106 a non-developable shape, yarns have to be tied to one another. They can be woven,
107 stitched or knitted. Four kinds of reinforcements have been tested in this study. All are
108 used in aeronautical applications and enable to manufacture thick parts.

109 The first considered example of dry reinforcement is an 2.5D carbon fabric (fig. 1). Its
110 area weight is 630 g/m^2 and the thickness is 1 mm. It will be denoted "fabric A".

111 The second example of dry reinforcement is an interlock carbon fabric G1151® (fig. 2).
112 It is a laminate of four layers. Its area weight is 600 g/m^2 , the thickness is 0.6 mm
113 and it has 7.4 yarns/cm in warp way and 7.4 yarns/cm in weft way. It will be denoted

114 "fabric B".

115 The third example of dry reinforcement (fig. 3) is a carbon non crimp fabric (NCF) [30].

116 It will be denoted "fabric C". It is a laminate of two unidirectional plies with yarn
117 orientation at $\pm 45^\circ$ and plies tied by warp stitching. The area weight is 568 g/m^2 and
118 the thickness is 1.1 mm. In general, such reinforcement will be characterized by the
119 number of plies, orientation of plies, dimensions of the yarns, the pattern of the stitch
120 (chain or tricot) and its dimensions.

121 To increase the number of plies, it is possible to assemble several NCF reinforcements
122 and to stitch them with another stitching yarn (fig. 4). A fourth sample has been
123 tested. It will be denoted "fabric D". It is a multiply composed of two monoplies of
124 the previous NCF "fabric C". Its nominal area weight is 1230 g/m^2 .

125 With such structures, dry reinforcements can support high geometrical transformations
126 under low forces because the yarns are free to move. The mechanical behaviour which
127 results from this freedom of movement is specific and gives to the structure low rigidities
128 compared to those of tension in yarn directions. Because warp and weft yarns are joined
129 by weaving or stitching, the tensile behaviour is biaxial and tensile tests results have
130 been studied in several papers [31, 32]. Moreover, reinforcement forming on a double
131 curvature shape is possible by in-plane shear strains. Thereby, in-plane shear behaviour
132 has been thoroughly studied and corresponding tests have been developed [21].

133 2.2 Bending properties

134 Classically, bending behaviour of continuous shell is derived from the in-plane proper-
135 ties of the material. But Yu et al. [24] investigated the bending behaviour of a woven
136 preform through a cantilever experiment and simulation where the deflection was only

137 due to gravity. The authors showed the discrepancy between the experimental and
138 numerical results and concluded that bending rigidity derived from in-plane properties
139 gives unrealistically high value compared to the experimental bending rigidity of the
140 woven preform. During deformations, a part of the yarn will have its curvature increas-
141 ing while another part will have its curvature decreasing, involving interactions between
142 filaments and between yarns with high sliding. This multi-scale constitution gives to
143 the reinforcement a specific bending behaviour independent of the tensile or the shear
144 behaviour. For composite reinforcements, bending behaviour is a structural multi-scale
145 problem which cannot be directly deduced from the in-plane material properties and it
146 is then necessary to determine this specific behaviour. Up today, bending behaviour of
147 reinforcement has not been the subject of many researches. On the contrary, there are
148 a lot of studies in the field of clothing. Because of the similarity between the geometries
149 of textiles and reinforcement, the first idea was to examine the bending behaviour of
150 fabrics. The study of the bending behaviour of yarns or fabrics for the simulation means
151 defining the relationship between the moment M and the curvature κ of a bent beam,
152 plate or shell depending on the complexity of the model. Relationship between fabric
153 behaviour, structural configuration and mechanical behaviour of yarns and their con-
154 stituent fibers is complex and a critical review has been proposed by Ghosh et al. [33].
155 Another way is to define a macroscopic model based on rheological and experimental
156 measurements. The simplest macroscopic model is the linear elastic (eq. 1) proposed
157 by Peirce [34].

$$M = B \cdot \kappa \tag{1}$$

158 But Grosberg et al. proposed a more realistic model (eq. 2) [35] taking into account
 159 the hysteretic behaviour of the fabric with the frictional restraint couple M_0 :

$$\begin{cases} \kappa & = 0 & \text{if } M < M_0 \\ B \times \kappa & = M - \text{sign}(\kappa) \cdot M_0 & \text{if } M \geq M_0 \end{cases} \quad (2)$$

160 Recently, Ngo Ngoc et al. [36] and Lahey [37] proposed models based on mechanical
 161 friction theory to fit experimental data. In both ways, mesoscopic or macroscopic ap-
 162 proach, it is necessary to dispose of a bending test to verify the model. Although there
 163 are many methods to test the bending behaviour of a material, reinforcement with
 164 low bending stiffness needs specific equipment. Historically, it is again in the field of
 165 clothing textiles that such bending tests have been designed to evaluate the quality of
 166 fabrics. The two more common tests are presented in the next section.

167 3 Standard bending tests

168 3.1 Cantilever test

169 Peirce was the first to present both a macroscopic measurement of the bending be-
 170 haviour [34] and a mesoscopic approach [25] to model the geometric configuration of
 171 the mesh. Assuming an elastic linear behaviour between the bending moment and the
 172 curvature of the strip, he proposed a cantilever test (fig. 5) to determine the bending
 173 stiffness. In this test the fabric is cantilevered under gravity.

174 In his model, bending moment M (N.m) is a linear function of the curvature κ (m^{-1}):

$$M = G \times b \times \kappa \quad (3)$$

175 where G (N.m) is the flexural rigidity per unit width and b (m) is the width of the
 176 strip. Peirce defined the ratio S of the flexural rigidity to the weight w per unit area:

$$S = G/w \quad (4)$$

177 Assuming the fabric being an elastica and small strains but large deflections, he defined
 178 the relation between the ratio S , the angle θ of the chord with the horizontal axis and
 179 the length l of the bent part of the sample (fig. 5)

$$S = \frac{l^3}{8} \cdot \frac{\cos \theta/2}{\tan \theta} \quad (5)$$

180 The cubic root of S allows to compare the fabrics. It has the unit of a length and is
 181 called by Peirce "the bending length". Today, the standard commercial apparatus are
 182 defined with a specific value equal to 41.5° for the angle of the tilted plane. With this
 183 value, the equation (5) becomes simpler:

$$S \approx l^3/8 \quad (6)$$

184 This configuration is described in standard tests [26,27].

185 On this principle, Grosberg [35,38] proposed a cantilever test to determine the both
 186 parameters of his model (eq. 2). Considering two specific values of θ ($\theta = 40^\circ$ and
 187 $\theta = 20^\circ$) and assuming the load as a concentrated and a distributed load, the param-
 188 eters are computed using functions derived from known solutions.

189 Lastly, Clapp et al. [39] developed an indirect method of experimental measurement
 190 of the moment-curvature relationship for fabrics based on recording the coordinates of
 191 the deformed sample. Applying least square polynomial regression and numerical dif-
 192 ferentiation techniques, moment-curvature relationship is computed from coordinate
 193 data and weight per unit width. This method allows taking into account the non linear
 194 behaviour but assumes elastic behaviour.

195 3.2 KES -FB bending test

196 Kawabata's Evaluation System was originally designed to measure basic mechanical
 197 properties of fabrics [28]. It became a set of standard tests for tensile, shear, com-
 198 pression, surface roughness and bending behaviour. KES-FB tester (fig. 6) is the test
 199 to quantify properties in pure bending deformation mode and enables then to record
 200 directly the evolution of the bending momentum per unit width versus the curvature
 201 during a load unload cycle.

202 The dimension of the sample in the bending direction is equal to 1 cm and its width
 203 is 20 cm for flexible fabrics. It is clamped between a fixed (A) and a moving (B)
 204 clamps (fig. 6). The fixture setting of the sample in the clamps ensures pure bend-
 205 ing deformation. During the test, the moving clamp (B) rotates round the fixed one
 206 (A) ensuring a constant curvature through the sample length. The movement is made
 207 with a constant rate of curvature equal to $0.5 \text{ cm}^{-1}\text{s}^{-1}$ from -2.5 cm^{-1} to 2.5 cm^{-1} .
 208 As indicated in the manual of the apparatus, the bending rigidity B and the bending
 209 hysteresis M_0 of Grosberg's model are computed as follow: the slopes are computed re-
 210 spectively between $\kappa = 0.5 \text{ cm}^{-1}$ and $\kappa = 1.5 \text{ cm}^{-1}$ for s_1 and between $\kappa = -0.5 \text{ cm}^{-1}$
 211 and $\kappa = -1.5 \text{ cm}^{-1}$ for s_2 (see eq. 7).

$$\begin{cases} s_1 = \frac{\Delta M = M(\kappa=1.5) - M(\kappa=0.5)}{\Delta \kappa = 1} \\ s_2 = \frac{\Delta M = M(\kappa=-0.5) - M(\kappa=-1.5)}{\Delta \kappa = 1} \\ B = (s_1 + s_2)/2 \end{cases} \quad (7)$$

212 The bending hysteresis, that is the frictional restraint force M_0 , is the half average
 213 of the two hysteresis values h_1 and h_2 computed respectively at $\kappa = 1 \text{ cm}^{-1}$ and

214 $\kappa = -1 \text{ cm}^{-1}$ (see eq. 8).

$$\begin{cases} h_1 &= M_l(\kappa = 1) - M_{ul}(\kappa = 1) \\ h_2 &= M_l(\kappa = -1) - M_{ul}(\kappa = -1) \\ 2 \cdot M_0 &= (h_1 + h_2)/2 \end{cases} \quad (8)$$

215 where M_l and M_{ul} are respectively the moment for load and unload curve.

216 Figure 7 presents the results of the KES-FB test carried out on fabric A in weft
217 direction. The Grosberg's curve is drawn on the figure and the parameters are presented
218 in table 1. In this example, bending moment is in gf.cm/cm ($1 \text{ gf} \simeq 1 \text{ cN}$) and curvature
219 is in cm^{-1} .

220 This experimental bending test was developed for flexible textiles and testing stiff
221 or thick reinforcements requires to reduce length of the sample. Finally, it is neither
222 possible to test stiffer multiply reinforcements nor to easily observe the behaviour in
223 the thickness.

224 4 New flexometer

225 4.1 General description

226 Within standard testers (cantilever, KES-FB and other less known ones) cantilever
227 principle has been retained for a new flexometer because of its simplicity and flexibility
228 to test different reinforcements.

229 This new flexometer is constituted by two modules: a mechanical module and an optical
230 module. The mechanical module enables to place the sample in cantilever configuration
231 under its own weight. It is also possible to add a mass at the free edge of the sample
232 to reach larger curvatures. The optical module takes pictures the shape of the bent
233 sample. The sample can be a yarn, a monoply or multiply reinforcement. It has a

234 length about 300 mm and a width up to 150 mm. The thickness can reach several
235 millimeters.

236 At the beginning of the test (fig. 8(a)), the sample (S) is placed upon a fixed board (F)
237 and a special plane comprising laths (B). The length direction of the sample must be
238 parallel to the bending direction and its free edge must be aligned with the lath (L1).

239 A translucent plate (C) is fixed upon the both to ensure the embedding condition.

240 Thus the sample (S) will not slide. During the test, because of the translation of
241 the drawer (T), the laths will successively retract, beginning with lath (L1), and the

242 length of overhang will increase. The test is stopped for a chosen overhang length L

243 and is continued for new lengths. Thus, the complete test is a succession of quasi-
244 static tests with different loading cases. While single cantilever test provided only one

245 configuration, the new flexometer, with its set of loading cases associated with the
246 different bent shapes, enables to identify a non elastic behaviour model.

247 Like in several studies of textile deformability during composite processing [40] full-field
248 strain measurements are applied to measure the deformed shape of the bent sample. A
249 digital camera takes a picture for each length and the images are processed to extract

250 the shapes of the bent sample (fig. 8(b)). A previous step of pixel calibration [41] is
251 required so that pixel measurements can be translated into real dimension by scaling.

252 Then, the image of the bent sample profile is captured, filtered [42], and binarized. The

253 following step is to extract the borders of the binary object and to deduce the mean
254 profile (see fig. 9).

255 4.2 Post processing

256 At the end of the experimental test, a set of bent shapes is provided. Each bent shape
 257 is defined by the bending length at which the deformed shapes has been obtained and
 258 by the data points defined in a coordinate system. The subsequent post-processing of
 259 the profiles aims to deduce from them the evolution of the moment with the curvature.
 260 Each shape of the bent sample, defined by a set of data points, is smoothed by a
 261 series of exponential functions plus a first order polynomial to ensure the boundary
 262 conditions at embedded point. For each length of bending test, bending moment and
 263 the curvature have to be computed along the profile and moment-curvature graph can
 264 be drawn.

265 Assuming the sample as a shell with its length $L_0 = L$ in initial configuration, the new
 266 length is noted L_b in bent configuration. The total strain energy U_t is the summation
 267 of the bending energy U_b , the membrane strain energy U_m , and the transverse shear
 268 energy U_{TS} . In this case, assuming that the bending moment $M(s)$, the axial stress
 269 $N(s)$ and the transverse shear $T(s)$ are the only non zero stress components and that
 270 they depend only on the curvilinear abscissa s (see fig. 10) along the profile:

$$\kappa = \frac{z''}{(1 + z'^2)^{3/2}} \quad (9)$$

$$L_b = \int_{x_E}^{x_F} \sqrt{1 + z'^2} dt \quad (10)$$

$$s(P) = \int_{x_E}^{x_P} \sqrt{1 + z'^2} du \quad (11)$$

$$M(s) = W \int_s^{L_b} (u - s) \cos(\varphi) du \quad (12)$$

271 P defined by the curvilinear abscissa $s = s(P)$ is the point where the bending moment
 272 $M(s)$ applied by the part PF and the curvature *kappa* are computed. W is the weight
 273 per unit length (N/m). u and φ are the Frenet's coordinates of the point Q moving

274 along the shape from P to F.

$$\begin{cases} U_t = U_b + U_m + U_{TS} \\ U_t = \int_0^{L_b} M(s) \cdot \kappa(s) ds + \int_0^{L_b} N(s) \cdot \varepsilon_s(s) ds + \int_0^{L_b} T(s) \cdot \gamma(s) ds \end{cases} \quad (13)$$

275 Assuming that we are in pure bending deformation the membrane strain energy is
 276 insignificant by comparison with the bending energy, it follows that membrane strains
 277 are negligible and that bent length L_b is equal to initial length L . Finite element
 278 simulation of this bending test has been developed, in good agreement on the bending
 279 deflection value and confirms this hypothesis that membrane strains are negligible [43].

$$U_b = \int_0^L M(s) \cdot \kappa(s) ds \quad (14)$$

$$L_b = L \quad (15)$$

280 4.3 Test interpretation

281 Three curves are deduced of the experimental test (fig. 11):

- 282 – $M(L)$ (fig. 11(a)): each curve presents the evolution of the bending moment applied
 283 at a material point with the bending length.
- 284 – $\kappa(L)$ (fig. 11(b)): each curve presents the evolution of the curvature of the shape
 285 at a material point with the bending length.
- 286 – $M(\kappa)$ (fig. 11(c)): this curve is obtained by combination of the both previous. It
 287 presents the evolution of the moment with the curvature as the actual behaviour
 288 of the material.

289 Two points of the shape, P and Q are followed to illustrate the interpretation. During
 290 the test, points which are before the embedded point have a zero bending moment and
 291 a zero curvature: before L_P for P and before L_Q for Q. With increasing length of over-
 292 hang, when a point becomes the embedded point ($L = L_P$ for P), its moment becomes

293 equal to the resultant bending moment due to the bent part of the sample. Length
294 of overhang continues to increase and this point has its bending moment decreasing
295 because of the increasing inclination of the bent part.

296 Thus, when Q becomes the embedded point ($L = L_Q$), moment has already decreased
297 for point P. For each material point, its moment reaches maximum value when it be-
298 comes the embedded point and decreases after. Assuming an increasing relationship
299 between moment and curvature, which seems to be realistic, the curvature reaches also
300 its maximum value at the embedded point and decreases after (see curve $\kappa(L)$).

301 If the material has an elastic behaviour, load and unload curves of the moment-
302 curvature graph are superposed (curve $m(\kappa)$). In this case P and Q go up and down
303 along the elastic curve (continuous line). Thus, only one length of overhang, that is
304 only one bent shape, will be sufficient [39].

305 For non elastic and nonlinear behaviour (fig. 11) the locus of the points which have the
306 moment and curvature at their maximum values (at the embedded point) gives the load
307 part of moment-curvature curve (continuous line). On the other hand, following the
308 moment and the curvature for a material point will give the unload curve (dash line).
309 It is then necessary to test the bending behaviour with several lengths of overhang.

310 This explanation points out the difference between the new flexometer with its com-
311 plete test and the simple standard cantilever test. The standard test enables to provide
312 only bending rigidity for linear elastic model if only one point of the shape is exploited.
313 It enables to provide the parameters of a non linear but elastic model if the complete
314 shape is processed. But it does not enable to provide parameters for non elastic model
315 contrary to the new flexometer which takes into account the history of the deforma-
316 tions and enables then to identify non elastic models.

317 Moreover, each point has its maximum value of bending moment when it is the em-

318 bedded point (E). From equations (12) and (15), it follows that this value depends on

319 L:

$$M(E) = W \int_0^L s \cos(\varphi) ds \quad (16)$$

320 Each point undergoes a load at a maximum value increasing with the bending length
321 and an unload. During the unload phase, the behaviour could be different in function
322 of the level of load and in function of the material behaviour. For example, the be-
323 haviour of the sample can be quasi elastic for low bending length (low curvature), and
324 can become strongly hysteretic with high bending length (high curvature). The new
325 flexometer test is then equivalent to a set of KES-FB tests with different ranges of
326 curvature.

327 In practice, after having deduced moment-curvature curve for each bending length,
328 we'll see if the curves are superposed. In this case we consider that the behaviour is
329 elastic¹ and the moment-curvature graph for the greatest length enables to define the
330 bending model. If not, the moment and the curvature computed at embedded point
331 for each length of bending test enable to plot a point on the moment-curvature load
332 graph as explained above.

333 5 Bending tests

334 5.1 Test on fabric A and validation of flexometer

335 A test has been performed on fabric A (sec. 2.1) on the new flexometer presented in
336 section 4 and compared with measurements performed on KES-FB (Kawabata Eval-
337 uation System) at ENSISA (Ecole Nationale Supérieure d'Ingénieurs Sud Alsace) of

¹ but non necessarily linear

338 Mulhouse.

339 For the flexometer, the sample's width is equal to 100 mm and the test has been per-
340 formed with the bent strip under its own weight only. The weft direction of the sample
341 was parallel to the bending direction of the flexometer. The usable bending length
342 varied from 100 mm to 210 mm. The first step within the results analysis is to verify
343 if the behaviour is linear elastic. For each bent shape, the angle θ of the chord with
344 the horizontal axis defined by Peirce's test has been determined (fig.5). It follows the
345 flexural rigidity G according to equations (4) and (5). If the behaviour is linear elastic,
346 this parameter should be constant. Figure 12 shows the evolution of this parameter
347 with the bending length L . It turns out that G decreases while the length increases.
348 With a variation of about 42 % (tab. 2), it can be inferred that the behaviour is not
349 linear² for the fabric considered.

350 Figure 13 shows the evolution of the moment with the curvature computed along the
351 profile for three lengths $L = 100$ mm, $L = 150$ mm and $L = 210$ mm. Moment is in
352 N (moment per unit width). Other lengths have been tested but they are not plotted
353 for more clarity. It can be observed inflexions for low curvatures which don't represent
354 physical reality but are due to wiggles of the smoothing function in quasi rectilinear
355 parts of the profiles. It ensues that the curve given for $L = 100$ mm may be not usable.
356 The curves seem to be superposed which could indicate a quasi-elastic behaviour. In
357 this case, the bending behaviour is described by the moment-curvature curve given for
358 the largest length as explained in section 4.3.

359 For each bending length, let curvature and moment computed at the embedded point
360 be considered. Curvature increases with the length increasing but changes very slowly
361 for length greater than 200 mm due to the low moment arm. For the largest length

² but it can be elastic nevertheless

362 it is around 0.045 mm^{-1} (fig. 14(a)). Concerning the maximum moment, it can be
363 noticed a little inflexion because of the decreasing moment arm and the softening
364 of the structure (fig. 14(b)). The combination of these both curves allows deducing
365 the loading curve. In the case of elastic behaviour, loading curve is superposed with
366 moment-curvature curve computed along the profile.

367 For the KES-FB bending test carried out on fabric A, the sample width has been
368 reduced to 3 cm instead of 20 cm to complete the test. Figure 7 shows the moment-
369 curvature graph recorded for a test performed on one of the samples. Figure 15 shows
370 the moment-curvature curve recorded during the test KES-FB and with the flexometer.
371 It can be noted that flexometer measurements are in good agreement with KES-FB
372 bending test. Due to the limitation on the KES system, it has been impossible to carry
373 out a complete test with another composite reinforcements (like two plies of fabric A,
374 nor with two plies of fabric C). We can conclude, as even, by these comparisons with
375 the KES-FB test, that in our experimental methodology, the flexometer test is validate.

376 5.2 Test with larger curvature

377 The second set of tests has been performed on fabric B (sec. 2.1). A first series of five
378 tests has been performed under their own weights only and in weft direction. The sam-
379 ples width was equal to 100 mm and the usable bending length varied from 100 mm
380 to 260 mm. Figure 16 show the repeatability of the deflection of the samples for three
381 lengths. The relative standard deviation of the maximal deflection undergoes a vari-
382 ation by 1 % for larger length to 19 % for smaller length. Another test of intrinsic
383 repeatability of the flexometer gave a relative standard deviation of the maximal de-
384 flection less than 0.2 % for large lengths and 5 % for small lengths. It follows that the

385 observed repeatability is essentially due to the material scattering.

386 The Peirce's rigidity variation shows again that the behaviour is not linear elas-
387 tic (tab. 3). Concerning the curvature (fig. 17(a)), it increases with the length in-
388 creasing with a more marked visible asymptotic behaviour. For the largest length it
389 reaches around 0.036 mm^{-1} . For the moment (fig. 17(b)), a change of slope can be
390 observed around $L = 190 \text{ mm}$. To complete the repeatability of the test, a study of
391 the scatterings of curvature indicated that the relative standard deviation is length
392 independent and comprised between 5 and 21 %. These large variations are due still to
393 the numerical double derivative of the smoothing exponential function (with wiggles)
394 to compute the curvature (sec. 4.2). In opposite, the relative standard deviation of
395 moment, between 1 and 5 %, is much less extensive because moment is computed by
396 integration.

397 A metal strip has been stuck on the free edge of the sample to reach larger curva-
398 tures in the second series of tests. This added mass increases the moment especially at
399 the beginning of the test for small bending lengths. Consequently the deformation of
400 the sample is accelerated. Test have been performed with strip which had the weight
401 equal to the two third of the sample weight. This time, the bending length varied from
402 50 mm to 240 mm. Figure 18 presents the moment versus the curvature computed
403 along the profiles for all the lengths for one of the samples. Using the mass, the max-
404 imum curvature can reaches the significant value of 0.15 mm^{-1} . It's an advantage of
405 our experimental system, with the possibility to add a mass in fact to reach large value
406 of the curvature, without changing the sample geometry. Moreover, it can be noted
407 larger range of curvature. The curves are divided into two sets. The curves of the first
408 set are superposed which indicates an elastic behaviour. In opposite, the curves split off
409 in the second set. The behaviour is non elastic. The behaviour changes for κ between

410 0.04 and 0.045 mm⁻¹.

411 Finally, figure 19 shows the averages of the loading curves (e.g. moment and curvature
412 computed at embedded point) for the two sets of tests (under own weight only and
413 with added mass) performed on fabric B. For the tests carried out under own weight
414 only, the curvature reaches 0.036 mm⁻¹ and the moment 0.11 N. The behaviour is only
415 elastic all over the range of curvature. For the tests carried out with added mass, the
416 curvature reaches 0.10 mm⁻¹ and the moment 0.12 N. The marked change of slope
417 confirms that the material change from an elastic behaviour to an inelastic at curvature
418 between 0.04 and 0.045 mm⁻¹. It can be observed a good continuity between the two
419 series (without and with added mass).

420 5.3 Non Crimped Fabric bending test

421 Another test has been performed on a fabric C (Non Crimp Fabric) presented in sec-
422 tion 2.1. The sample had its width equal to 50 mm. The test has been performed with
423 the bent strip under its own weight only. The results are presented for bending lengths
424 between 100 mm and 170 mm. Because moment-curvature computed along the profiles
425 indicated a non elastic behaviour, bending moment and curvature have been computed
426 at the embedding point. These results are directly presented in the figure 20. From low
427 curvatures, points seem to be in an asymptotic zone and the moment increases very
428 little. The non woven structure should enable the fibers and the yarns to slide widely.
429 Because the behaviour seems to be inelastic from the low curvatures and assuming an
430 hysteretic behaviour, Dahl's model [44] can be chose to fit with the moment-curvature
431 curve using least square method. This model is used by Ngo Ngoc et al. to fit on KES
432 bending tests performed on clothing textiles [36]. It is very efficient for clothing tex-

433 tiles and it could be a good starting point for reinforcements. The bending curve is
 434 defined by a differential equation where moment is only curvature dependent and rate
 435 independent:

$$\frac{dM}{d\kappa} = B_0 \left(1 - \frac{M}{M_0} \text{sign}(\dot{\kappa}) \right) \quad (17)$$

436 The optimization of Dahl's model gives $B_0 = 6.11$ N.mm and $M_0 = 0.040$ N.
 437 A second test has been performed on fabric D (2 stitched multiplies of fabric C). The
 438 sample's width is 100 mm. The test has been performed with the bent strip under its
 439 own weight only. The results are presented for bending length between 100 mm and
 440 170 mm. Bending moment and curvature have been computed at the embedding point
 441 and reported on the figure 20. This time, first points seem to be in an increasing zone
 442 while last points seem to have reached asymptotic zone. Assuming again an hysteretic
 443 behaviour, the Dahl's model has been chosen to fit with the experimental curve and
 444 the optimization gives $B_0 = 8.92$ N.mm and $M_0 = 0.104$ N. With two plies, the initial
 445 bending rigidity B_0 increases by 45 % and the asymptotic momentum M_0 increases
 446 by 160 %. In the case of elastic linear shell hypothesis without in-plane shear strain,
 447 the bending rigidity should have increased by cubic variation of thickness. If both
 448 of the plies were free to slide completely, the bending rigidity would be near to the
 449 value of one ply. Because of the warp stitch, the plies are not completely free to slide
 450 and the bending behaviour of the multiply results of the bending behaviour of the
 451 structural monoply plus frictional interactions between the two plies and action of the
 452 stitch. However, again because of the difficulty to compute the curvature, data points
 453 are scattered and the question arises as to whether Dahl's model is suitable for the
 454 reinforcement considered.

455 **6 Conclusion**

456 Bending behaviour of composite reinforcements is going to become a significant be-
457 haviour to take into account in forming processes simulations, especially in case of
458 the simulation of out-of-plane phenomenon during these processes, like the wrinkles.
459 This behaviour is a specific complex multi-scale mechanical problem. At macroscopic
460 scale bending behaviour is described by the constitutive moment curvature relation-
461 ship which is not linear and depends on the range of the curvature. Whatever the
462 scale used to approach the problem, a macroscopic bending test is warranted to verify
463 the model and identify experimentally the behaviour. Present standard bending tests
464 designed for clothing textiles are not adequate for composite reinforcements. Thereby,
465 a new cantilever test has been designed to test various reinforcements with different
466 thicknesses, different woven structures and with low or large bending rigidity. In the
467 new flexometer test, optical measure and image processing accurately provide cartesian
468 coordinates of the deformed sample for each bending length. From these, a first direct
469 method enables to plot the moment-curvature graph. Contrary to the classical can-
470 tilever test, the flexometer test is operated with several bending lengths which allows
471 obtaining non linear non elastic bending behaviour because the test takes into account
472 the history of the deformation. Moreover, a complete flexometer test is equivalent to
473 multiple KES-FB tests with different ranges of curvature because KES-FB tests only
474 one point with only one history while the new flexometer tests a set of points with
475 different histories of load.

476 A first test performed on the same kind of reinforcement both with new flexometer and
477 KES-FB tester allowed to validate the new test method. The second set of tests showed
478 that the repeatability of the position of the shape ensued from natural repeatability of

479 the material but it pointed out also the extensive uncertainties of curvature because
480 of the numerical double derivative computation. This highlights the limit of the direct
481 method. A set of tests with an added strip stuck to the free edge allowed to access
482 to larger curvature and to identify the change from elastic to non elastic behaviour.
483 Finally tests performed on monopoly and multiply allowed to compare their bending
484 properties. These last tests have shown that the flexometer enables to test thicker and
485 stiffer reinforcements than KES-FB apparatus.

486 Associated to this experimental development this study permits us to show the limits
487 of the bending models developed for clothing textile, when they are used for composite
488 reinforcement. The loads are significantly higher in composite materials applications
489 than in the clothing industry, the constitution and the rigidity are different and conse-
490 quently models for deformation of woven fabrics as developed for the clothing industry
491 are often not applicable for composites [45]. The definition of a specific model concerns
492 ours futures works for the bending behaviour. This definition will be associated to an
493 inverse method built on experimental results and results obtained by the simulation of
494 the bending test by finite element method. The aim of inverse method is to optimize the
495 parameters of the chosen model, by minimizing the gap between experimental shape
496 and simulated shape.

497 **Acknowledgements** The authors thank Laurence Schacher of the Laboratoire de Physique
498 et Mécanique Textiles de Mulhouse (ENSISA) to have allowed us to perform the KES bending
499 tests. The authors acknowledge also the support of the ITOOL European project.ŠIntegrated
500 Tool for Simulation of Textile CompositesŠ, European Specific Targeted, Research Project,
501 SIXTH FRAMEWORK PROGRAMME, Aeronautics and Space, <http://www.itool.eu>.

Table 1 Grosberg's parameters computed on KES-FB test carried out on fabric A

s_1 (gf.cm)	s_2 (gf.cm)	B (gf.cm)
3.95	3.40	3.68
h_1 (gf)	h_2 (gf)	M_0 (gf)
6.44	5.04	2.87

Table 2 Flexometer test on fabric A. Variation of flexural rigidity G with bending length L .

G_{min}	G_{max}	G_{moy}	$\Delta G = \frac{G_{max}-G_{min}}{G_{moy}}$ (%)
4,49	6,78	5,42	42,3
(N.mm)			(%)

Table 3 Flexometer test on fabric B. Variation of flexural rigidity G with bending length L .

G_{min}	G_{max}	G_{moy}	$\Delta G = \frac{G_{max}-G_{min}}{G_{moy}}$ (%)
6,16	11,07	8,84	55,6
(N.mm)			(%)

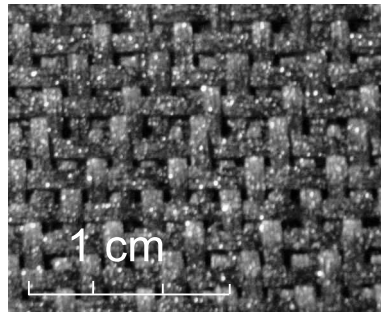


Fig. 1 Fabric A = 2.5D carbon fabric

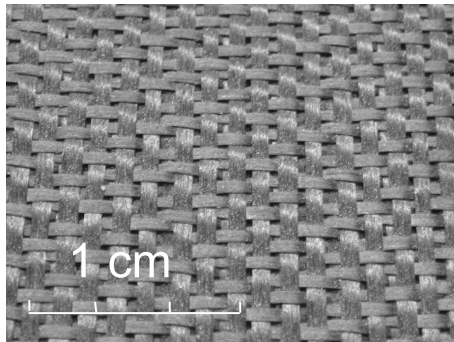
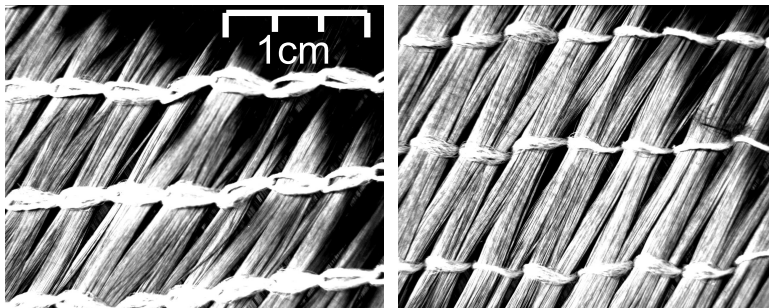


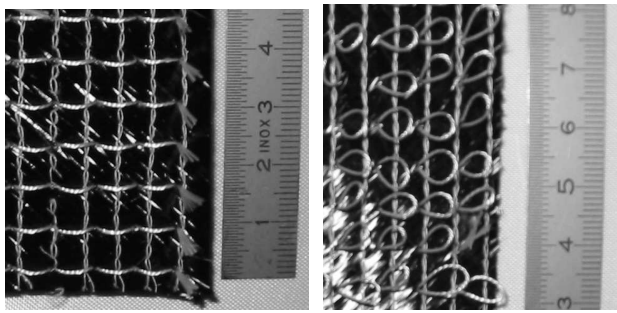
Fig. 2 Fabric B = interlock carbon fabric, G1151@



(a) Top

(b) Bottom

Fig. 3 Fabric C = carbon Non Crimp Fabric (NCF)



(a) Top

(b) Bottom

Fig. 4 Fabric D = Multiply Non Crimp Fabric (2 plies of fabric C)

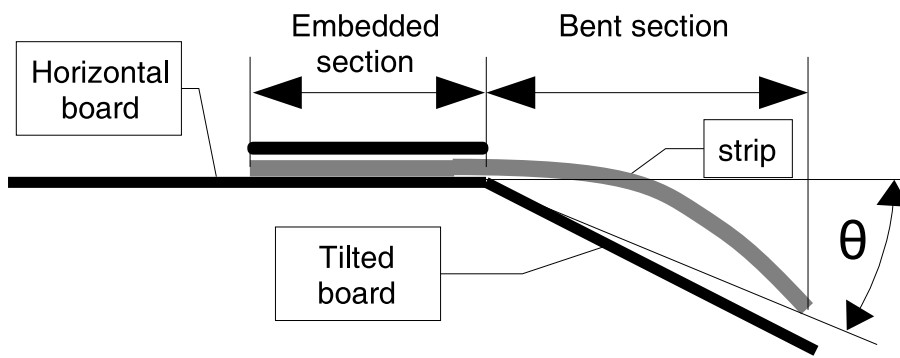


Fig. 5 The cantilever test for fabric: The Peirce's test is without the tilted board and the length of overhang is constant and θ is variable. With the standard cantilever test, the sample slides until it touches the tilted board at $\theta = 41.5^\circ$. The length of overhang is variable and θ is constant.

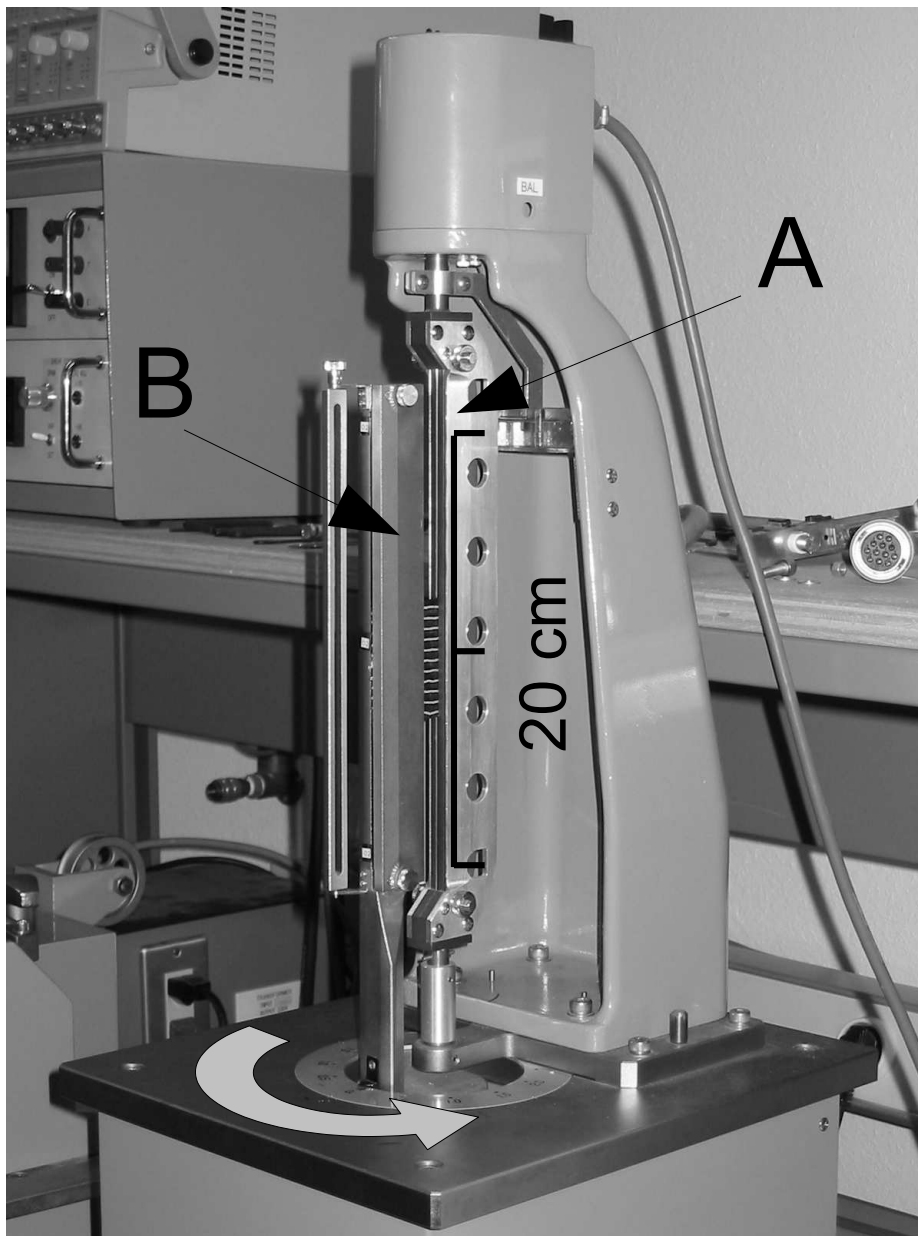


Fig. 6 Kawabata bending test - KES-FB2 / ENSISA Mulhouse

BENDING

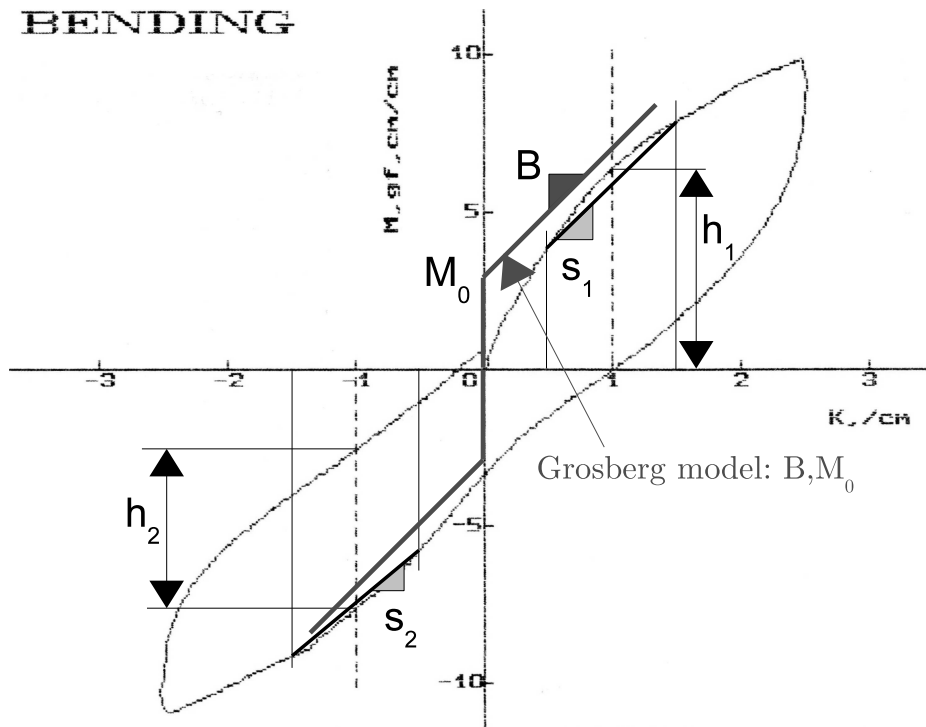
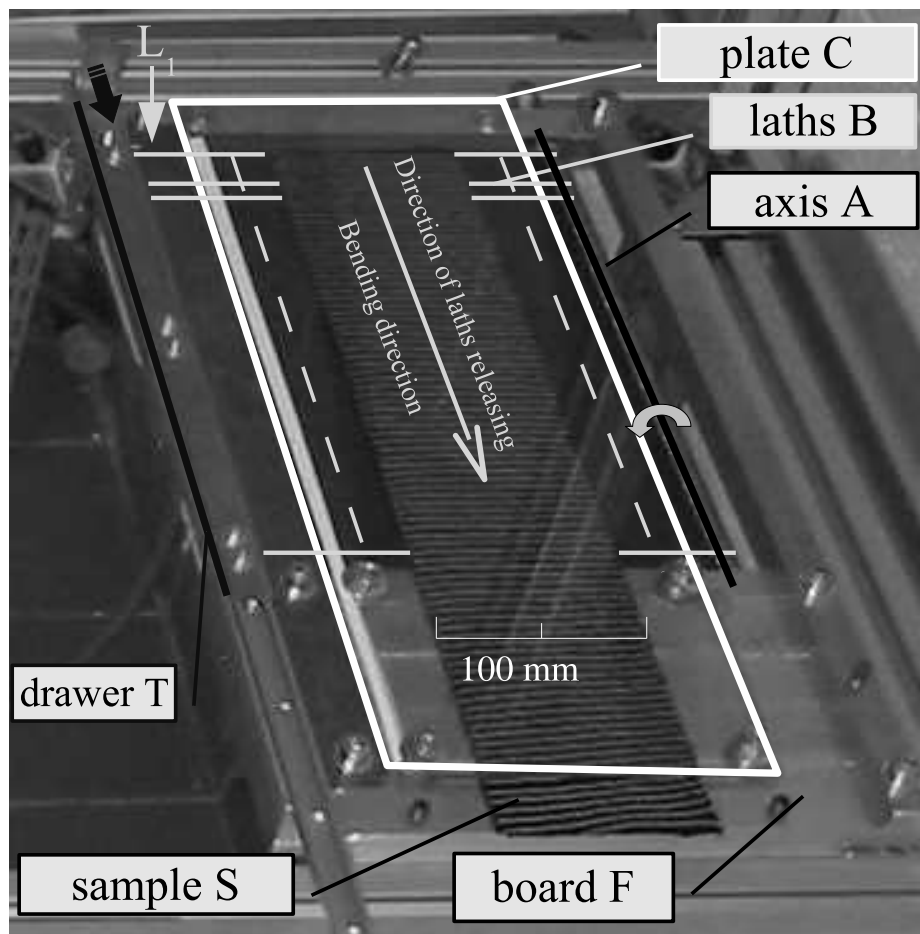
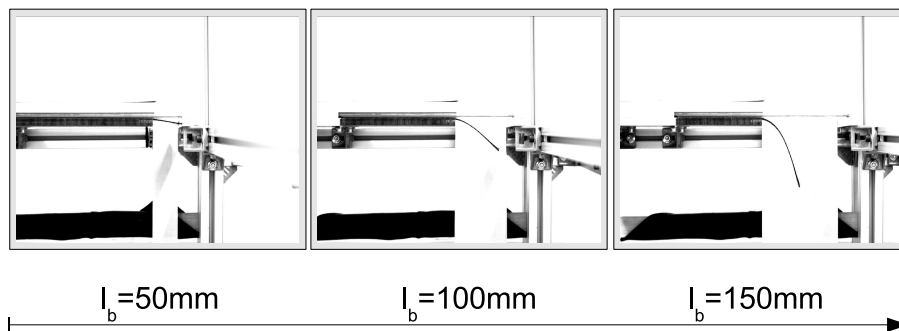


Fig. 7 KES FB2 test data carried out on fabric A and Grosberg's parameters



(a) Flexometer - Mechanical module with sample



(b) Three successive bending lengths measurements during a test. Pictures taken by optical module

Fig. 8 New flexometer based on cantilever test with successive bending lengths

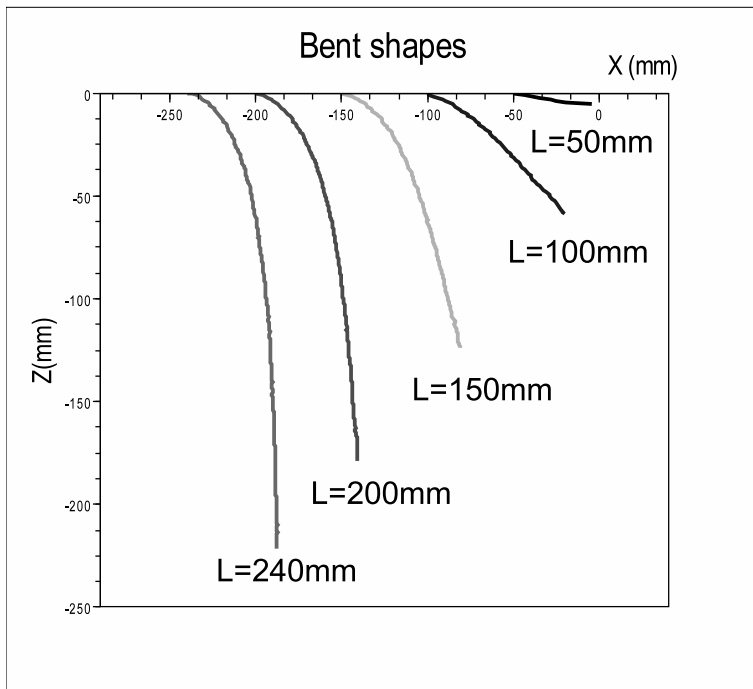


Fig. 9 Flexometer test - For each bending length, a profile is extracted from the picture by image processing.

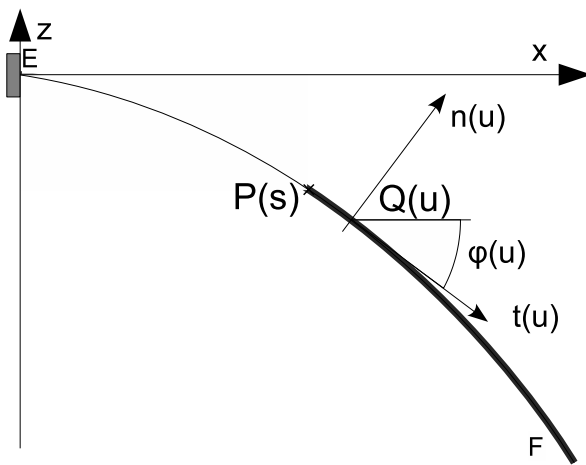


Fig. 10 Bending moment computing along the profile. E is the embedded point. F corresponds to the free edge. Curvature and moment are computed at general point P with curvilinear abscissa s

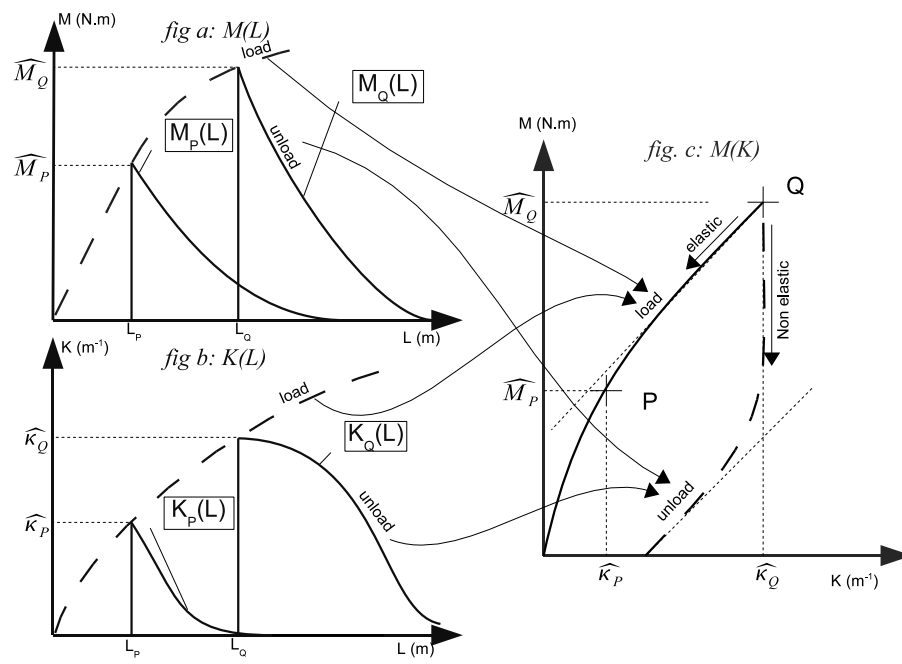


Fig. 11 Flexometer - Test interpretation. Elastic and non elastic behaviour

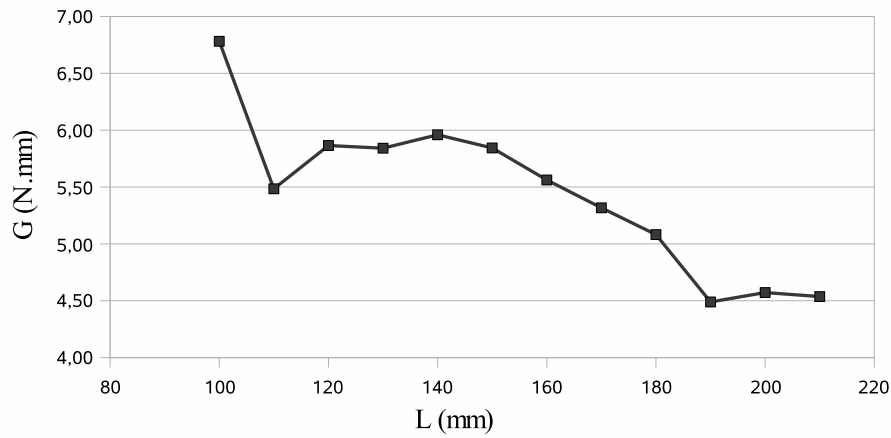


Fig. 12 Flexometer test on fabric A. Evolution of flexural rigidity G with bending length L .

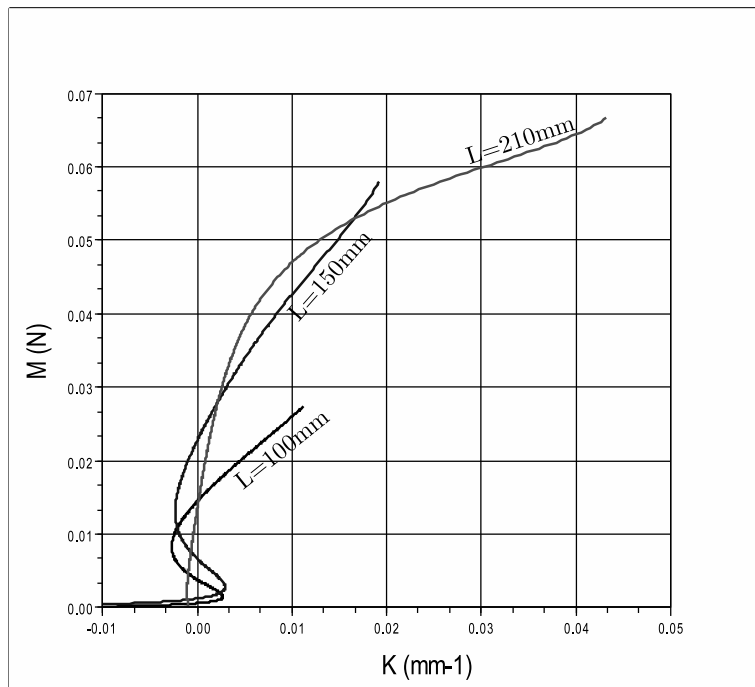
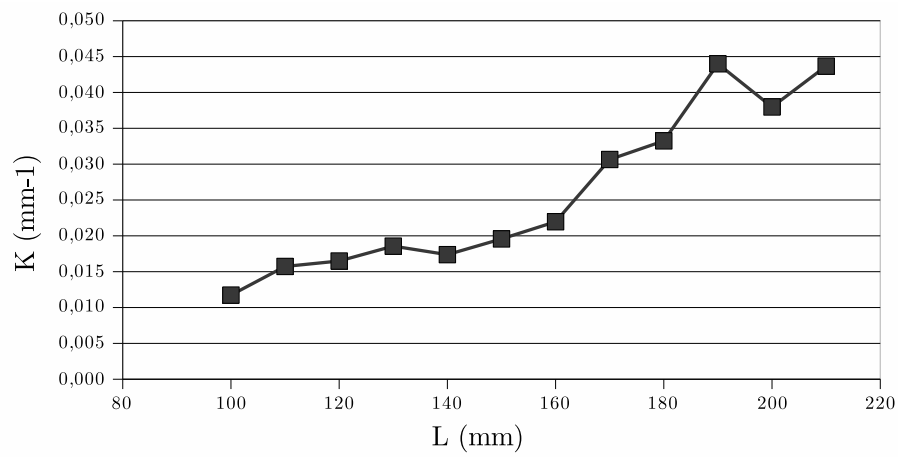
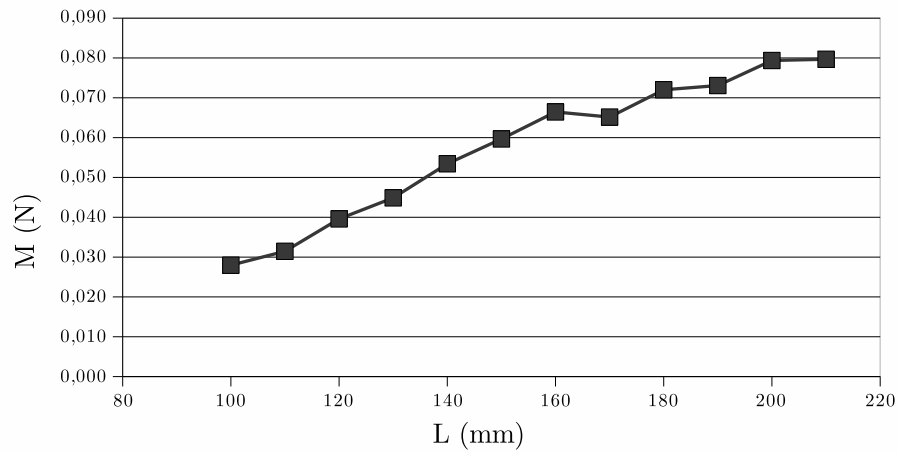


Fig. 13 Flexometer test on fabric A. Moment-curvature computed along the profiles for $L = 100$ mm, $L = 150$ mm and $L = 210$ mm.



(a) Curvature vs Bending length



(b) Moment vs Bending length

Fig. 14 Flexometer test on fabric A. Curvature and moment computed at embedded point vs Bending length

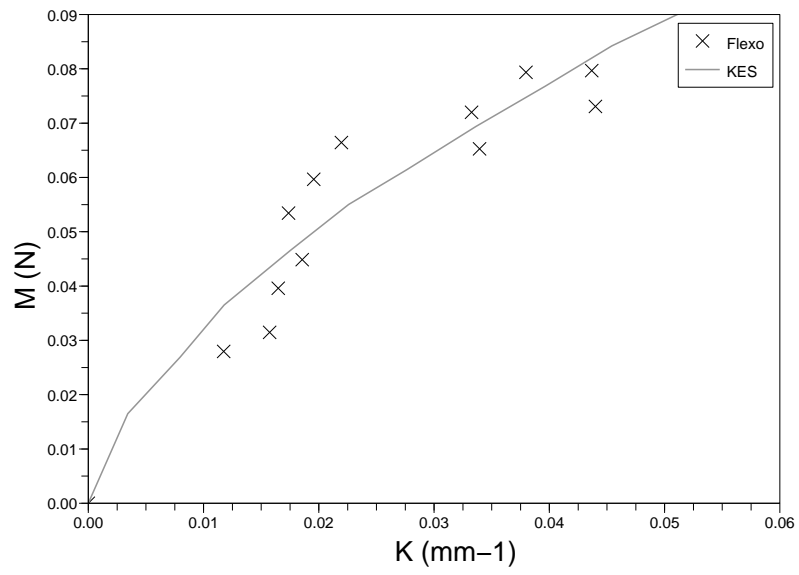
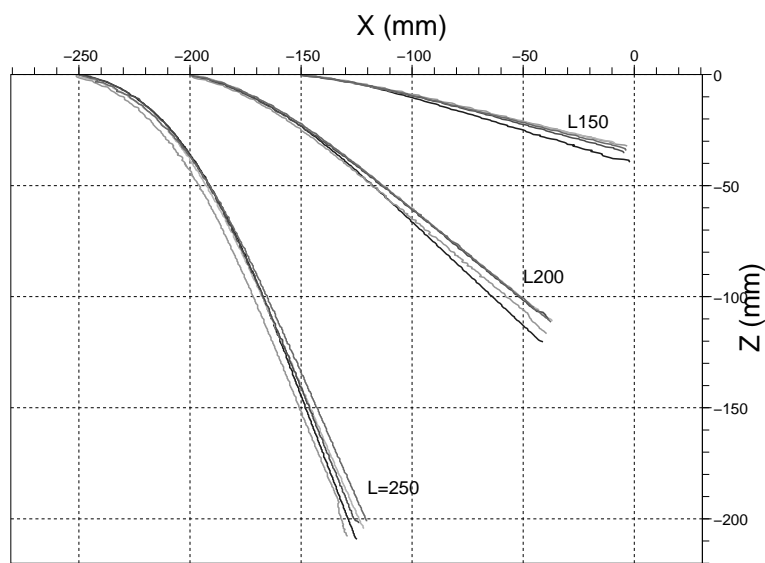
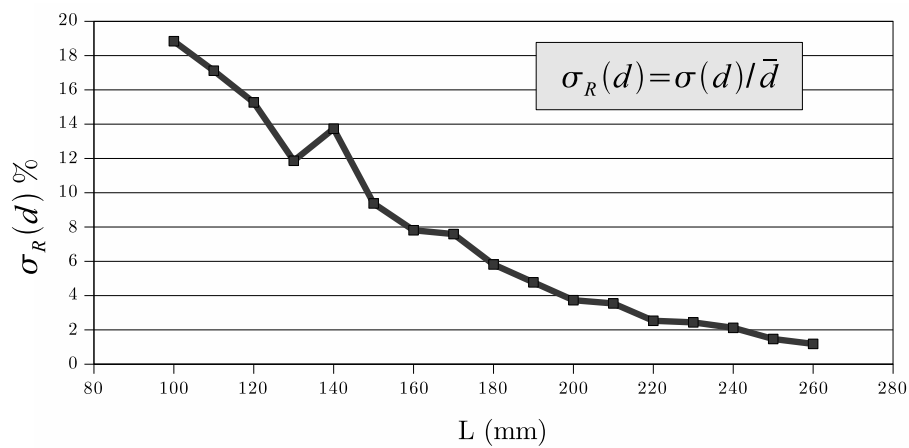


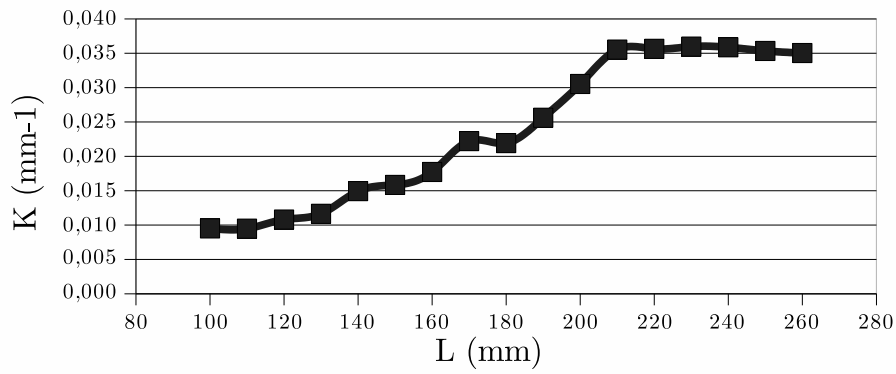
Fig. 15 Bending curve for fabric A - Comparison with Flexometer test and KES-FB2



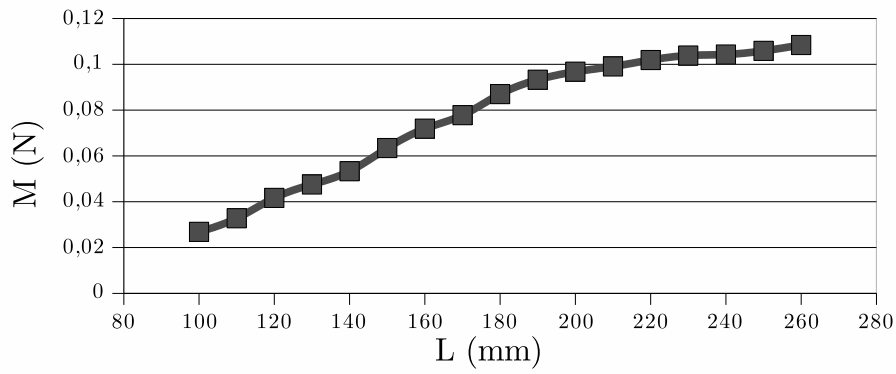
(a) Profiles

(b) Repeatability of maximal deflection ($d = Z$ co-ordinate of free edge F)**Fig. 16** Flexometer test on fabric B. Repeatability on the reinforcement for bending lengths

$L = 150$ mm, $L = 200$ mm et $L = 250$ mm



(a) Curvature vs Bending length



(b) Moment vs Bending length

Fig. 17 Flexometer test on fabric B. Curvature and moment computed at embedded point vs Bending length

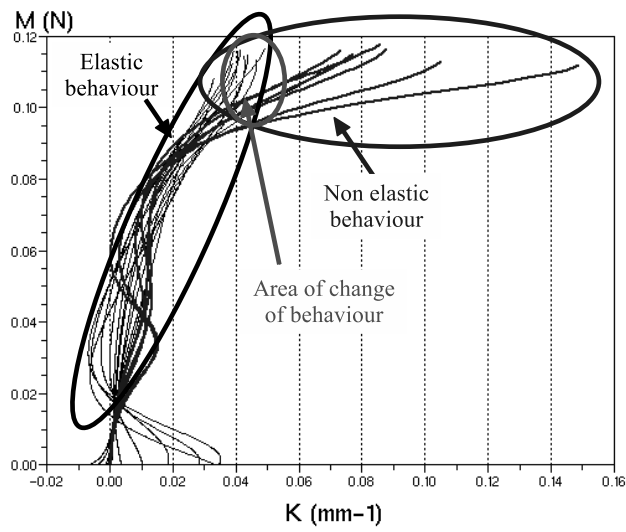


Fig. 18 Flexometer test on fabric B with added mass. Curvature and moment computed along profiles vs bending length.

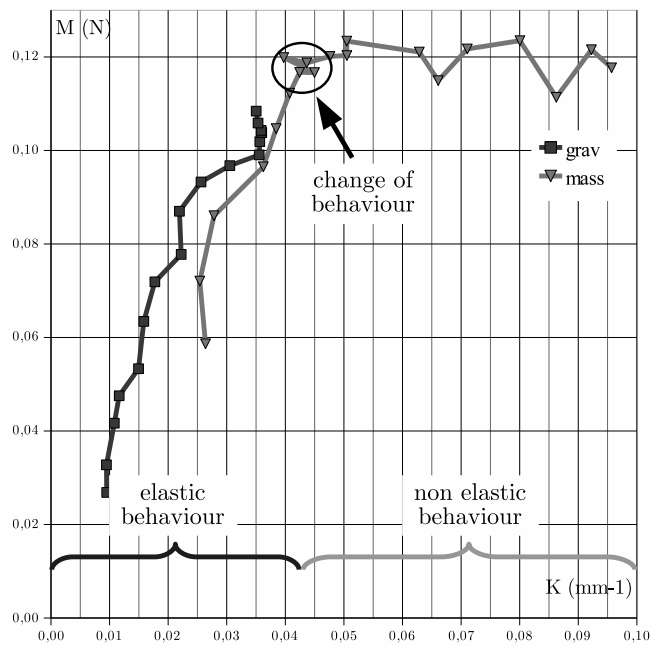


Fig. 19 Bending curve for fabric B under gravity and with added mass.

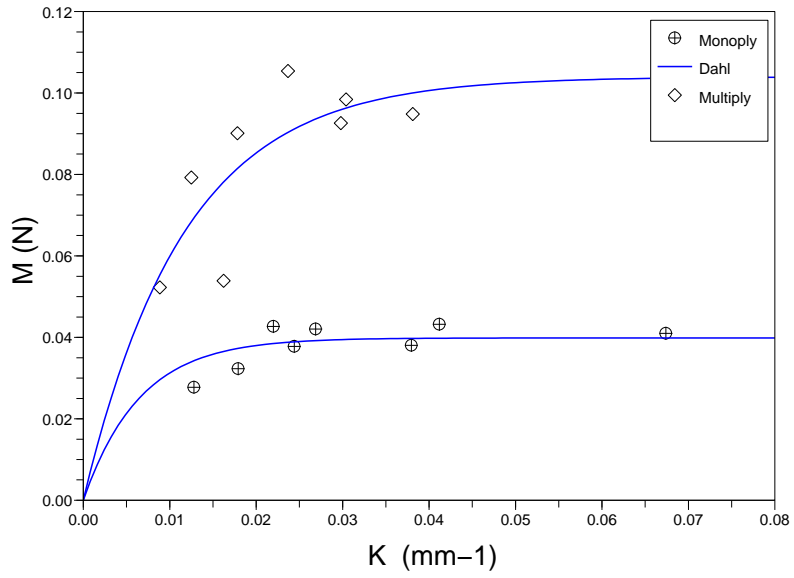


Fig. 20 Bending curve for fabric C (NCF) and fabric D (Multiply NCF).

502 References

- 503 1. Long, A.: Design and manufacture of textile composites. Woodhead Publishing Ltd (2005)
- 504 2. Rudd, C., Long, A., Kendall, K., Mangin, C.: Liquid Moulding Technologies. Woodhead
505 Publishing (1997)
- 506 3. Potter, K.: The early history of the resin transfer moulding process for aerospace applica-
507 tions. *Composites Part A: Applied Science and Manufacturing* **30**(5), 619–621 (1999)
- 508 4. Parnas, R.S.: Liquid composite molding. Hanser Gardner Publications (2000)
- 509 5. Maison, S., Thibout, C., Garrigues, C., Garcin, J., Payen, H., Sibois, H., Coiffer, C.,
510 Vautey, P.: Technical developments in thermoplastic composites fuselages. In: SAMPE
511 journal, 5, pp. 33–39 (1998)
- 512 6. Soulat, D., Cheruet, A., Boisse, P.: Simulation of continuous fibre reinforced thermoplastic
513 forming using a shell finite element with transverse stress. *Computers and structures* **84**,
514 888–903 (2006)
- 515 7. Long, A., Rudd, C.D.: A simulation of reinforcement deformation during the production
516 of preforms for liquid moulding processes. ARCHIVE: Proceedings of the Institution of
517 Mechanical Engineers, Part B: Journal of Engineering Manufacture 1989-1996 (vols 203-
518 210) **208**(42), 269–278 (1994)
- 519 8. Pillai, K., Advani, S.: The role of dual permeability of fiber preforms in resin transfer mold-
520 ing. In: Proceedings of the American Society for Composites Ninth Technical Conference
521 (1994)
- 522 9. Rudd, C., Long, A., McGeehin, P., Cucinella, F., Bulmer, L.: Processing and mechanical
523 properties of bi-directional preforms for liquid composite moulding. *Composites Manufac-*
524 *turing* **6**(3-4), 211–219 (1995)
- 525 10. Advani, S., Brusckke, M., Parnas, R.: Flow and Rheology in Polymeric Composites Man-
526 ufacturing, chap. 12 - Resin transfer molding. Elsevier Publishers (1994)
- 527 11. Rudd, C., Middleton, V., Owen, M., Long, A., McGeehin, P., Bulmer, L.: Modelling the
528 processing and performance of preforms for liquid moulding processes. *Composites Man-*
529 *ufacturing* **5**(3), 177–186 (1994)
- 530 12. Laroche, D., Vu-Khanh, T.: Forming of woven fabric composites. *Journal of Composite*
531 *Materials* **28**(18), 1825–1839 (1994)

-
- 532 13. Mark, C., Taylor, H.: The fitting of woven cloth to surfaces. *Journal of Textile Institute*
533 (1956)
- 534 14. Van Der Weeën, F.: Algorithms for draping fabrics on doubly-curved surfaces. *International*
535 *Journal for Numerical Methods in Engineering* **31**(7), 1415–1426 (1991)
- 536 15. Cherouat, A., Borouchaki, H., Billoët, J.: Geometrical and mechanical draping of compos-
537 ite fabric. *European Journal of Computational Mechanics* (2005)
- 538 16. Boisse, P., Zouari, B., Gasser, A.: A mesoscopic approach for the simulation of woven fibre
539 composite forming. *Composites Science and Technology* **65**(3-4), 429–436 (2005)
- 540 17. Boisse, P., Zouari, B., Daniel, J.: Importance of in-plane shear rigidity in finite element
541 analyses of woven fabric composite preforming. *Composites Part A: Applied Science and*
542 *Manufacturing* **37**, 2201–2212 (2006)
- 543 18. Zouari, B., Daniel, J., Boisse, P.: A woven reinforcement forming simulation method.
544 influence of the shear stiffness. *Computers & Structures* **84**(5-6), 351–363 (2006)
- 545 19. Boisse, P., Hamila, N., Helenon, F., Hagege, B., Cao, J.: Different approaches for woven
546 composite reinforcement forming simulation. *International Journal of Material Forming*
547 **1**(1), 21–29 (2008)
- 548 20. Hamila, N., Boisse, P.: Simulations of textile composite reinforcement draping using a new
549 semi-discrete three node finite element. *Composites Part B: Engineering* **39**(6), 999–1010
550 (2008)
- 551 21. Launay, J., Hivet, G., Duong, A., Boisse, P.: Experimental analysis of the influence of
552 tensions on in plane shear behaviour of woven composite reinforcements. *Composites*
553 *Science and Technology* **68**(2), 506–515 (2008)
- 554 22. Hamila, N.: Simulation de la mise en forme des renforts composites mono et multi plis.
555 Ph.D. thesis, Institut National des Sciences Appliquées de Lyon (2007)
- 556 23. Wang, J., Long, A., Clifford, M., Lin, H.: Energy analysis of reinforcement deformations
557 during viscous textile composite forming. In: E. Cueto, F. Chinesta (eds.) *AIP Conference*
558 *Proceedings*, vol. 907, pp. 1098–1106. AIP (2007)
- 559 24. Yu, W., Zampaloni, M., Pourboghra, F., Chung, K., Kang, T.: Analysis of flexible bending
560 behavior of woven preform using non-orthogonal constitutive equation. *Composite Part*
561 *A : Applied science and manufacturing* **36** (6), 839–850 (2005)

-
- 562 25. Peirce, F.: The geometry of cloth structure. *The Journal of the Textile Institute* **28**, 45–96
563 (1937)
- 564 26. ASTM: Standard Test Method for Stiffness of Fabrics, chap. D1388-96(2002). American
565 Society for Testing and Materials (2002)
- 566 27. ISO: Textiles glass -Woven fabrics - Determination of conventional flexural stiffness - Fixed
567 angle flexometer method, chap. ISO 4604:1978. ISO (1978)
- 568 28. Kawabata, S.: The standardization and analysis of hand evaluation. The Textile Machinery
569 Society of Japan (1980)
- 570 29. Hivet, G., Boisse, P.: Consistent 3d geometrical model of fabric elementary cell. application
571 to a meshing preprocessor for 3d finite element analysis. *Finite element in analysis and
572 design* **42**, 25–49 (2005)
- 573 30. Lomov, S., Belov, E., Bischoff, T., Ghosh, S., Truong Chi, T., Verpoest, I.: Carbon com-
574 posites based on multiaxial multiply stitched preforms. part 1. geometry of the preform.
575 *Composites Part A: Applied Science and Manufacturing* **33**(9), 1171–1183 (2002)
- 576 31. Boisse, P., Buet, K., Gasser, A., Launay, J.: Meso/macro-mechanical behaviour of textile
577 reinforcements for thin composites. *Composites Science and Technology* **61**(3), 395–401
578 (2001)
- 579 32. Boisse, P., Gasser, A., Hivet, G.: Analyses of fabric tensile behaviour: determination of
580 the biaxial tension-strain surfaces and their use in forming simulations. *Composites Part
581 A: Applied Science and Manufacturing* **32**(10), 1395–1414 (2001)
- 582 33. Ghosh, T., Batr, S., Barke, R.: The bending behaviour of plain-woven fabrics. part i : A
583 critical review. *The Journal of the Textile Institute* **81**, 245–254 (1990)
- 584 34. Peirce, F.: The 'handle' of cloth as a measurable quantity. *The Journal of the Textile
585 Institute* **21**, 377–416 (1930)
- 586 35. Grosberg, P.: The mechanical properties of woven fabrics part ii : the bending of woven
587 fabrics. *Textile Research Journal* **36** (3), 205–214 (1966)
- 588 36. Ngo Ngoc, C., BRUNIAUX, P., J.M., C.: Modelling friction for yarn/fabric simulation
589 application to bending hysteresis. In: *Proceedings 14th European Simulation Symposium*
590 (2002)
- 591 37. Lahey, J.T., Heppler, G.R.: Mechanical modeling of fabrics in bending. ASME (2004)

-
- 592 38. Grosberg, P., Kedia, S.: The mechanical properties of woven fabrics part i : the initial load
593 extension modulus of woven fabrics. *Textile Research Journal* **36** (1), 71-79 (1966)
- 594 39. Clapp, T., Peng, H., Gosh, T., Eischen, J.: Indirect measurement of the moment-curvature
595 relationship for fabrics. *Textile Research Journal* **60**(9), 525-533 (1990)
- 596 40. Lomov, S., Boisse, P., Deluycker, E., Morestin, F., Vanclooster, K., Vandepitte, D., Ver-
597 poest, I., Willems, A.: Full-field strain measurements in textile deformability studies. *Com-
598 posites Part A: Applied Science and Manufacturing* **39**(8), 1232-1244 (2008)
- 599 41. Bailey, D.: Pixel calibration techniques. In: *New zealand Image and Vision Computing 95
600 Workshop*, pp. 37-42 (1995)
- 601 42. Bailey, D.: A rank based edge enhancement filter. In: *New Zealand Image Processing
602 Workshop*, pp. 42-47 (1990)
- 603 43. de Bilbao, E., Soulat, D., Hivet, G., Launay, J., Gasser, A.: Bending test of composite
604 reinforcements. In: *ESAFORM 2008* (2008)
- 605 44. Dahl, P.: Solid friction damping of mechanical vibrations. *AIAA Journal* **14**(12), 1675-
606 1682 (1976)
- 607 45. Prodromou, A.G., Chen, J.: On the relationship between shear angle and wrinkling of
608 textile composite preforms. *Composites Part A: Applied Science and Manufacturing* **28**(5),
609 491-503 (1997)